Inorganic Chemistry

Article

pubs.acs.org/IC

Solvent or Temperature Induced Diverse Coordination Polymers of Silver(I) Sulfate and Bipyrazole Systems: Syntheses, Crystal Structures, Luminescence, and Sorption Properties

Li-Yun Du,[†] Wen-Juan Shi,[†] Lei Hou,*[,†,‡] Yao-Yu Wang,[†] Qi-Zhen Shi,[†] and Zhonghua Zhu[‡]

[†]Key Laboratory of Synthetic and Natural Functional Molecule Chemistry of the Ministry of Education, Shaanxi Key Laboratory of Physico-Inorganic Chemistry, College of Chemistry & Materials Science, Northwest University, Xi'an 710069, People's Republic of China

[‡]School of Chemical Engineering, the University of Queensland, Brisbane 4072, Australia

Supporting Information

ABSTRACT: Three new coordination polymers, $[Ag_4(H_2bpz)_4(SO_4)_2]\cdot H_2O$ (**1**), $[Ag_2(H_2bpz)_2(SO_4)]\cdot 3H_2O$ (**2**), and $[Ag_3(H_2bpz)_4](SO_4)_{2/3}(OH)_{5/3}\cdot 4H_2O$ (**3**) have been solvothermally synthesized with Ag_2SO_4 and flexible ligand 3,3′,5,5′-tetramethyl-4,4′-bipyrazole (H_2bpz) in different solvents and temperatures. Complex **1** is a 2-fold interpenetrated three-dimensional (3D) framework with an uncommon (3,5)-connected hms topology. Complex **2** is a structural isomer of **1** and shows a three-connected 2D ths net consisting of interesting 3-fold and 2-fold heterochiral helical chains. Complex **3** discloses a grid layer structure, containing heterochiral helical chains and an unusual *meso*-helix. More interestingly, three sets of layers in **3** stack in different directions, affording an unprecedented 2D + 2D + 2D → 3D polycatenating cationic framework with 1D + 3D porous systems. In **1**−**3**, H_2bpz exhibit exobidentate bridging fashions with wide-ranged interpyrazole tilting angles and changeable coordination configurations, such as *cis* and *trans* fashions in **1** and **3** and uniform *trans* fashion in **2**. These lead to the isomeric $[Ag(H_2bpz)]_n$ arrays of wavelike and helical chains in **1** and **2**, respectively. Complexes **1**−**3** display solid-state photoluminescence stemming from the ligand-centered fluorescent emissions of H_2bpz. Because of the highly polar framework, **3** shows excellent adsorption selectivity for CO_2 over N_2.

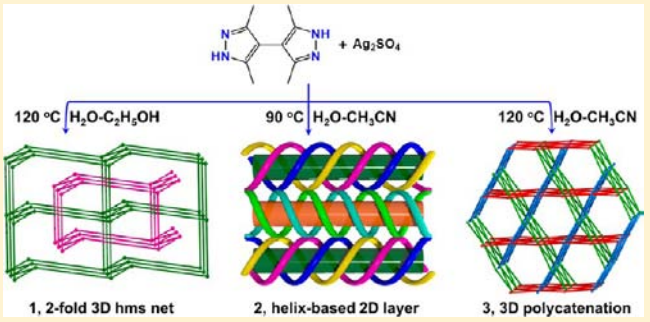

INTRODUCTION

Coordination polymer (CP) research is a fast-developing research area for academic and industrial applications.[1] In this context, numerous CPs were assembled by various approaches, such as combining the same organic ligands with different metal ions, introducing different anions, changing the substituent groups or lengths of organic ligands, incorporating mixed ligands, and so on. To date, it remains a considerable challenge to control the structures of CPs because many external factors, such as solvent systems, pH values, and temperatures impose crucial influences on the structures of compounds.[2] It is particularly attractive to build different CPs from the same reactants by controlling these external factors.[3]

Ag(I)-based CPs have gained intensive attention because of intriguing structures and outstanding functional properties in sorption, conductive materials, luminescence, antibacterial uses, and sensing devices.[4] Scientists observed that the anions exerted important effects on the structures of Ag(I) complexes. While most of them focused on the monovalent anions, such as NO_3^-, BF_4^-, ClO_4^-, PF_6^-, $CF_3SO_3^-$ and $CF_3CO_2^-$,[5] only a few involved other coordinated anions, especially for SO_4^{2-} dianion. Besides as a counteranion, SO_4^{2-} often serves as a bridging ligand to form polymeric structures.[6] Although SO_4^{2-} exhibits multiple coordination modes, only 33 Ag(I) complexes containing SO_4^{2-} ligand were documented according to the latest CCDC research (version 5.34). The possible reason is the insolubility of Ag_2SO_4 in common solvents, which makes it difficult for the formation/crystallization of complexes. Therefore, the construction of diverse CPs from Ag_2SO_4 and the same ligand is a challenging and interesting project.

3,3′,5,5′-Tetramethyl-4,4′-bipyrazole (H_2bpz) features considerable flexibility, in which two pyrazolyl rings can rotate freely around the central C−C bond with interplanar angles of 50−90°,[7] leading to the fact that the distances of two metal centers and the angles of two metal−pyrazole bonds for one H_2bpz vary in wide ranges (Scheme 1). Moreover, H_2bpz can adopt a *cis* or *trans* coordination configuration. Consequently H_2bpz has a changeable bridging orientation and can diversify the dimensionalities and topologies of CPs. Several 1D, 2D, and 3D Ag(I)−H_2bpz CPs have been prepared through incorporating different anions, such as NO_3^-, $PO_2F_2^-$, ClO_4^-, $CF_3SO_3^-$,

Received: July 9, 2013
Published: December 2, 2013

   dx.doi.org/10.1021/ic401765r | Inorg. Chem. 2013, 52, 14018−14027

Scheme 1. The Different Coordination Configurations of H_2bpz

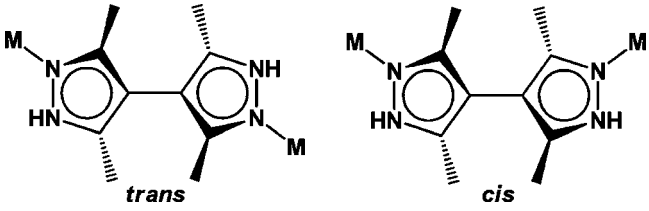

$CF_3CO_2^-$ and $H_2PO_4^-$,[5b,8] in which, depending on the configurations of H_2bpz, the $[Ag(H_2bpz)]_n$ polymeric arrays exhibit linear or helical chains. If SO_4^{2-} anion is introduced in Ag(I)−H_2bpz systems, diverse CPs are securable. So far, no related investigation has been undertaken.

Much effort has been devoted to preparing porous CPs (PCPs) as CO_2 capture and separation materials.[9] However, the major known porous frameworks are subjected to poor chemical stability, such as structural collapse or distortion in water or even moisture.[9b,10] Because of the great robustness of metal−pyrazole coordination bonds, the pyrazole-based PCPs display good thermal stability and resistance toward water and organic solvents.[11] Meanwhile, the pyrazole -NH groups of H_2bpz in frameworks can produce strong affinity for CO_2 molecules,[12] which enhance sorption selectivities for CO_2 over other gases. In addition, unlike other metal ions, few Ag(I)-based PCPs were engaged in the gas sorption investigations,[13] though the low-coordinated Ag(I) centers as exposed Lewis acid sites can attract CO_2 molecules. We herein present three new CPs, $[Ag_4(H_2bpz)_4(SO_4)_2]\cdot H_2O$ (**1**), $[Ag_2(H_2bpz)_2(SO_4)]\cdot 3H_2O$ (**2**), and $[Ag_3(H_2bpz)_4](SO_4)_{2/3}(OH)_{5/3}\cdot 4H_2O$ (**3**), which were synthesized by solvothermal reactions of Ag_2SO_4 and H_2bpz in different solvents and temperatures. Structures, luminescence, and sorption properties were investigated.

EXPERIMENTAL SECTION

Materials and General Methods. Commercially available reagents were used as received. H_2bpz was synthesized according to published procedures.[14] Infrared spectra (IR) were recorded from 4000 to 650 cm^{-1} with a PerkinElmer Spectrum 100 instrument. Elemental analyses of C, H, and N were determined with a PerkinElmer 2400C elemental analyzer. Photoluminescence analyses were performed on an Edinburgh FLS55 luminescence spectrometer. Thermal gravimetric analyses (TGA) were carried out in air stream using a PerkinElmer STA 6000 thermal analyzer at a heating rate of 5 °C/min. Powder X-ray diffraction (PXRD) data were recorded on a Bruker D8 ADVANCE X-ray powder diffractometer (Cu Kα, 1.5418 Å). Sorption isotherms were measured using a Micrometrics Tristar 3020 instrument. Samples were activated under vacuum at 130 °C for 5 h to remove solvent molecules prior to measurements.

Systhesis of $[Ag_4(H_2bpz)_4(SO_4)_2]\cdot H_2O$ (1). A mixture of Ag_2SO_4 (0.031 g, 0.1 mmol) and H_2bpz (0.019 g, 0.1 mmol) in ethanol (2 mL) and H_2O (7 mL) was stirred for 20 min. The solution was placed in a Teflon-lined stainless steel vessel (15 mL); the vessel was sealed and heated at 120 °C for 72 h, and then slowly cooled to room temperature. Colorless block crystals of **1** were isolated by filtration, washed with ethanol and H_2O, and dried in air. The yield was ca.15 mg (42.8%). Anal. Calcd for $C_{40}H_{58}Ag_4N_{16}O_9S_2$: C, 34.25; H, 4.17; N, 15.98. Found: C, 34.31; H, 4.11; N, 15.93. IR (cm^{-1}): 3147w, 2921w, 1559w, 1419m, 1300m, 1131m, 1091m, 1071s, 1023vs, 966w, 770m.

Systhesis of $[Ag_2(H_2bpz)_2(SO_4)]\cdot 3H_2O$ (2). Complex **2** was prepared in a similar procedure to that for **1**, by using acetonitrile (2 mL) instead of ethanol and reaction temperature of 90 °C. Colorless prism crystals were obtained in ca. 37.8% yield (14 mg). Anal. Calcd for $C_{20}H_{34}Ag_2N_8O_7S$: C, 32.19; H, 4.59; N, 15.01. Found: C, 32.15; H, 4.64; N, 14.95. IR (cm^{-1}): 3373w, 3156w, 2916w, 1640w, 1568w, 1463w, 1423w, 1307m, 1100s, 1043vs, 977w, 853w, 778m.

$[Ag_3(H_2bpz)_4](SO_4)_{2/3}(OH)_{5/3}\cdot 4H_2O$ (3). Complex **3** was prepared in a similar procedure to that for **1**, by replacing ethanol with acetonitrile (2 mL). Colorless sheet crystals were obtained in ca. 47.4% yield (15 mg). Anal. Calcd for $C_{40}H_{65.67}Ag_3N_{16}O_{8.33}S_{0.67}$: C, 38.46; H, 5.30; N, 17.94. Found: C, 38.52; H, 5.24; N, 17.89. IR (cm^{-1}): 3159w, 2925m, 1627w, 1555m, 1419m, 1299m, 1078s, 1025vs, 971w, 864w, 777m.

Table 1. Crystallographic Data of 1−3

	1	2	3
empirical formula	$C_{40}H_{58}Ag_4N_{16}O_9S_2$	$C_{20}H_{34}Ag_2N_8O_7S$	$C_{40}H_{56}Ag_3N_{16}O_{2.67}S_{0.67}$
formula wt	1402.62	746.35	1148.66
cryst syst	triclinic	orthorhombic	trigonal
space group	*P*1	*Ccca*	*P*3*c*1
T (K)	296(2)	296(2)	296(2)
a (Å)	11.3533(15)	10.0707(9)	20.0120(17)
b (Å)	11.4578(15)	24.215(3)	20.0120(17)
c (Å)	12.932(3)	26.085(3)	25.273(3)
α (deg)	109.471(2)	90.00	90.00
β (deg)	101.616(2)	90.00	90.00
γ (deg)	112.420(2)	90.00	120.00
V (Å^3)	1358.0(4)	6361.3(11)	8765.4(14)
Z	1	8	6
D_c (g cm^{-3})	1.715	1.559	1.306
μ (mm^{-1})	1.562	1.344	1.063
reflns collected	7335	16 395	45 190
reflns unique	6236	3134	11 504
R(int)	0.0209	0.0571	0.0839
GOF	1.050	1.035	1.007
R_1[a], wR_2[b] [$I > 2\sigma(I)$]	0.0532, 0.1381	0.0547, 0.1454	0.0704, 0.1576
R_1, wR_2 (all data)	0.0672, 0.1536	0.0961, 0.1700	0.1139, 0.1800

[a] $R_1 = \sum||F_o| - |F_c||/\sum|F_o|$. [b] $wR_2 = [\sum w(F_o^2 - F_c^2)^2/\sum w(F_0^2)^2]^{1/2}$.

dx.doi.org/10.1021/ic401765r | *Inorg. Chem.* 2013, 52, 14018−14027

X-ray Crystallographic Measurements. Diffraction data were collected with Mo Kα radiation (λ = 0.71073 Å) at 296(2) K on a Bruker-AXS SMART CCD area detector diffractometer. Absorption corrections were carried out utilizing SADABS routine. The structures were solved by the direct methods and refined by full-matrix least-squares refinements based on F^2.[15] All non-hydrogen atoms were refined anisotropically. The hydrogen atoms were added to their geometrically ideal positions. OH^- anions and solvent molecules in **3** are highly disordered and could not be identified from the difference Fourier map; their contributions were therefore removed from the refinement using the SQUEEZE routine in PLATON.[16] Final formulas were determined by combining single-crystal structures, elemental microanalyses, and TGA. Relevant crystallographic data are given in Table 1.

GCMC Simulation Methodology. Grand canonical Monte Carlo (GCMC) simulations were performed for the adsorption of CO_2 in **3** at 298 K under different pressures (0.1 and 100 kPa) by the Sorption module of Material Studio.[17] The framework and the individual CO_2 molecule were considered to be rigid. The partial charges for carbon and oxygen atoms of CO_2 molecules were 0.576*e* and −0.288*e*, respectively.[18] The partial charges for atoms of **3** were derived from Qeq method and QEq_neutral1.0 parameter (Table S3, Supporting Information). One unit cell was used during the simulations. The interaction energies between CO_2 and framework were computed through the Coulomb and Lennard-Jones 6−12 (LJ) potentials. All parameters for CO_2 molecule and atoms of **3** were modeled with the universal forcefield (UFF) embedded in the MS modeling package. A cutoff distance of 12.5 Å was used for LJ interactions, and the Coulombic interactions were calculated by using Ewald summation. For each run, 1×10^7 steps were used for equilibrium followed by another 1×10^7 steps for production with the metropolis Monte Carlo simulation method.

RESULTS AND DISCUSSION

Synthesis. The formation and crystallization of CPs are closely correlated to the external experimental environment, such as solvents and temperatures, which determine the solubilities of reactants.[3a,b] Complexes **1**−**3** failed to form at room temperature because of the insolubility of Ag_2SO_4 in common solvents. In contrast, **1**−**3** were successfully synthesized by solvothermal reactions in different solvents or temperatures (Scheme 2). Reaction of the same initial reactants

Scheme 2. Various Products from Ag_2SO_4 and H_2bpz Reactants in Different Conditions

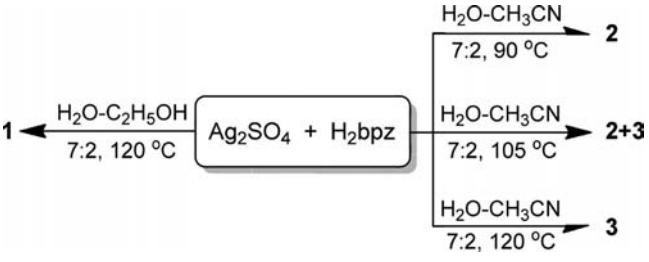

in different solvents or at different temperatures can generate diverse structures, which may provide direct evidence of the structural influence from these external factors. Complexes **1** and **3** were prepared at 120 °C in mixed water−ethanol (7:2) and water−acetonitrile (7:2) solvents, respectively. The different products mainly result from the different solubilities of Ag_2SO_4 and H_2bpz in water−ethanol and water−acetonitrile solvents. The yield of **3** was reduced with a decrease in synthesis temperature, such as at 105 °C; meanwhile, the prism crystals of **2** were gradually crystallized, and at 90 °C, pure crystals of **2** can be obtained. This result indicates that the formation of **2** and **3** is thermodynamically controlled. The higher ratios of Ag/H_2bpz in the formulas of **2** (1:1) than **3** (3:4) are possibly ascribed to the relatively low solubility of H_2bpz in water−acetonitrile solvent at 90 °C. Complexes **1**−**3** are stable in air, water, and common organic solvents. IR spectra demonstrate the characteristic $\nu_{S=O}$ vibrations of SO_4^{2-} at 1071 and 1091 cm^{-1} for **1**, 1100 cm^{-1} for **2**, and 1081 cm^{-1} for **3** (Figure S1, Supporting Information).

Crystal Structure of 1. Complex **1** crystallizes in the triclinic space group *P*1 and shows a 2-fold interpenetrated (3,5)-connected 3D framework. The asymmetric unit contains four independent Ag(I) ions, four H_2bpz, and two SO_4^{2-} anion ligands. As shown in Figure 1, all Ag atoms are three-coordinated by two pyrazole N atoms of two H_2bpz and one O atom of SO_4^{2-} anion, giving similar distorted T-shape geometries. The Ag atoms are alternately linked by H_2bpz to form a wavelike chain along the $(21\bar{1})$ direction (Figure 2a). The interpyrazole dihedral angles in H_2bpz are in range of 51.8−70.3°. Four distinct H_2bpz display exobidentate bridging coordinations with *cis* (N1- and N9-containing rings) and *trans* (N7- and N13-containing rings) configurations, which is unusual for a H_2bpz-based coordination polymeric chain in which only *cis*- or *trans*-H_2bpz was commonly presented.[5b,7,8a,19] The Ag···Ag distances separated by *trans*-H_2bpz (Ag1···Ag4 = 10.053 Å, Ag2···Ag3 = 9.939 Å) are longer than those in the *cis* ones (Ag1···Ag2 = 9.811 Å, Ag3···Ag4 = 9.345 Å). Two SO_4^{2-} anions in **1** show monodentate and tridentate coordinations, respectively, in which the latter plays an important role in the formation of 3D architecture. First, the interchain Ag2 and Ag3 atoms are dimerized by SO_4^{2-} anions with a *cis*−*cis* bridging mode to form a 2D layer parallel to the (201) plane. The intradimer Ag···Ag distance of 2.962 Å is much shorter than the sum of the van der Waals radii of two Ag atoms (3.40 Å), indicating strong metallophilic interactions. The layers are further pillared by another *trans*-bridged O atom of SO_4^{2-} anion along the (111) direction to form a 3D network, which has two types of tetragonal channels along the *b* and *c* axes, with the sizes of ca. 7.2 × 6.5 and 14.8 × 3.4 $Å^2$, respectively (Figures 2b). The large windows induce two identical frameworks interpenetrated, leaving 9.7% voids.[16] In addition, SO_4^{2-} anions are also involved in intra- and interframeworks N−H···O hydrogen bonds with uncoordinated pyrazole -NH groups of H_2bpz (Figure 3a, Table S2, Supporting Information), which stabilize the structure of **1**. This framework can be simplified as a (3,5)-connected hms net [point symbol $(6^3)(6^98)$],[20] upon consideration of the Ag_2 dimer and Ag4 atom as 5- and 3-connected nodes, respectively (Figure 3b). The hms topology is reported only in few CPs.[21]

Crystal Structure of 2. Complex **2** is a structural isomer of **1** due to the same framework components except differernt amounts of water guest molecules.[22] Complex **2** crystallizes in the orthorhombic space group *Ccca* and shows a helix-based layer structure. The asymmetric unit of **2** contains one Ag(I) ion, two H_2bpz, and one SO_4^{2-} anion lying in the 2-fold axes (Figure 4). Similar to **1**, the Ag atom in **2** also exhibits a three-coordinated T-shaped geometry defined by two pyrazole N atoms of two H_2bpz and one O atom of a SO_4^{2-} anion, as well as an exobidentate bridging coordinated H_2bpz with interplanar tilting angles of 57.7° and 70.0°. Differently, the interlinkages between H_2bpz and Ag atoms in **2** generate two symmetry-related left- and right-handed 4_1 helical chains along the *a* axis (Figure 5a). Similar $[Ag(H_2bpz)]_n$ helices were also observed in polymers $[Ag_4(H_2bpz)_5(NO_3)_4]$ and $[Ag(H_2bpz)]PO_2F_2$,[5b]

dx.doi.org/10.1021/ic401765r | Inorg. Chem. 2013, 52, 14018−14027

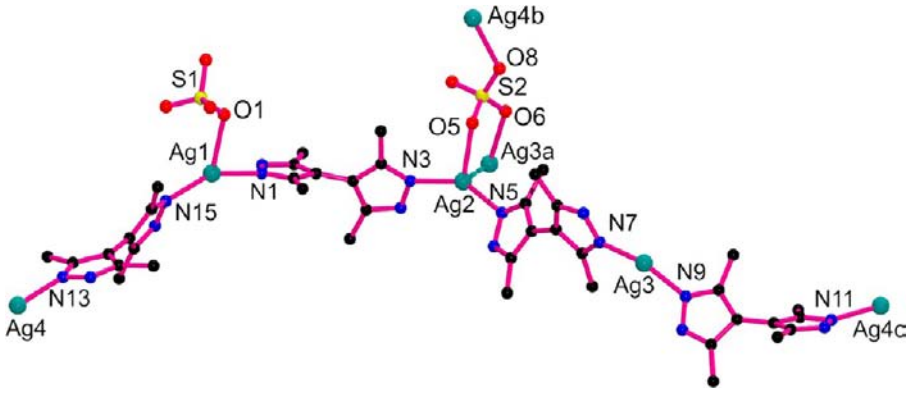

Figure 1. The coordination environments of Ag atoms in **1**. Symmetry codes: (a) x, $1 + y$, z; (b) $x - 2$, $y - 1$, z; (c) $x - 2$, $y - 2$, $1 + z$.

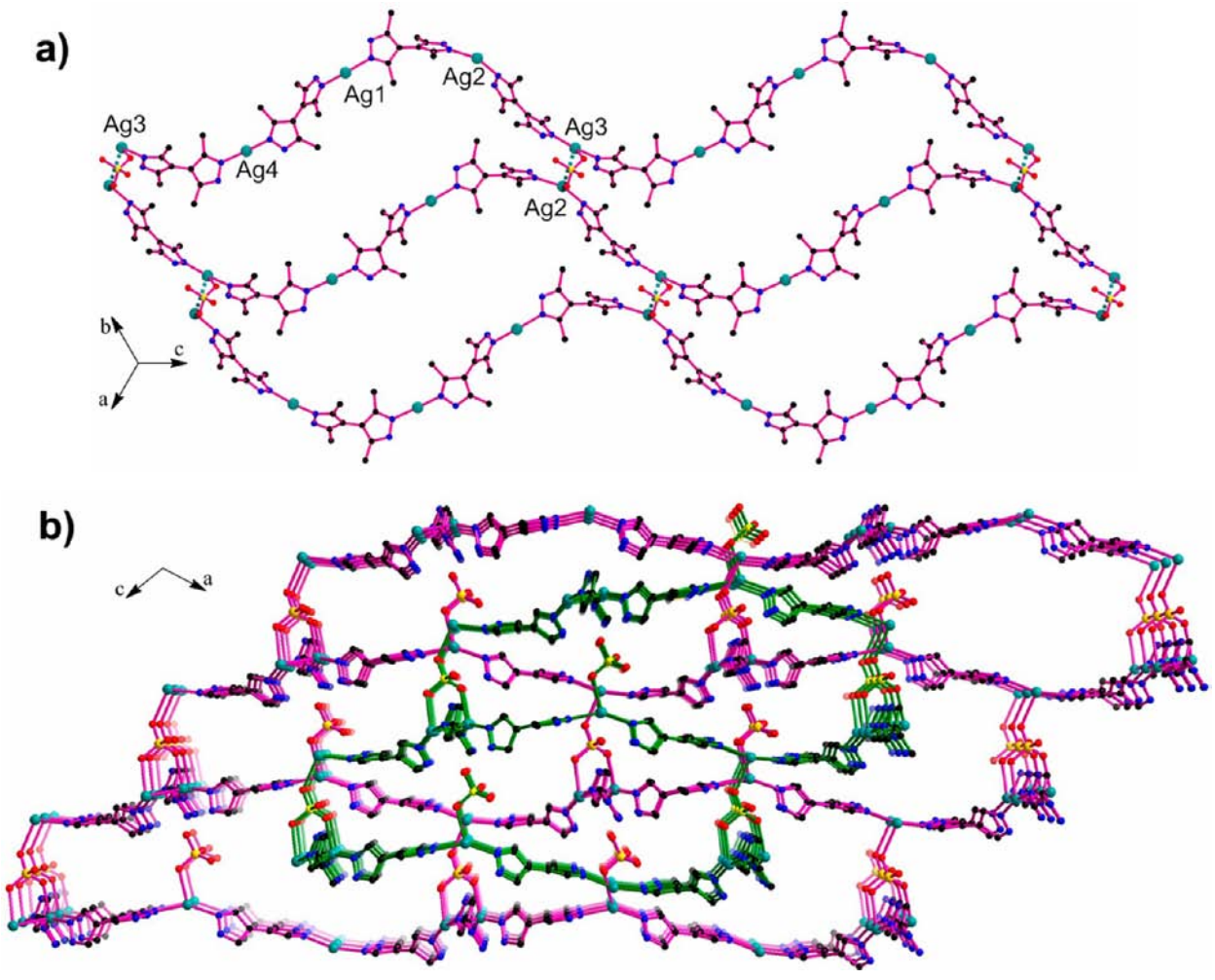

Figure 2. (a) Two-dimensional layer structure parallel to the (201) plane and (b) 2-fold interpenetrated framework of **1** viewed along the b axis.

which possess helical pitches of 24.9 and 23.9 Å, respectively, and show 2-fold helices. By contrast, the helix in **2** has an extra-long pitch of 30.212 Å (= 3c). As a result, an intriguing 3-fold helix is formed in **2** by associations of three homochiral helices, which represents the highest helical degree in known H_2bpz-incorporated complexes.

In **2**, SO_4^{2-} exhibits a bidentate *trans* bridging mode and links Ag atoms in adjacent helices along the b axis, forming a 2D layer parallel to the ab plane (Figure 5). In one layer, 3-fold helices have the same chirality; however, a 2-fold helix with the opposite chirality is formed between adjacent 3-fold helices, which contains a [Ag(H_2bpz)Ag(SO_4)] basic unit and a pitch of 20.141 Å (= 2c). The single layer is achiral and can be simplified as a 3-connected 10^3-ths net (Figure 6a), regarding both Ag and SO_4^{2-} as 3-connected nodes. Notably, 3-fold and 2-fold helices generate two types of helical channels along the a axis (Figure 6b), which feature hydrophobicity and hydrophilicity because their surfaces are occupied by methyl groups and methyl-SO_4^{2-} groups, respectively. Four water (O2W) guests form a $(H_4O)_4$ tetramer, which is anchored in the

dx.doi.org/10.1021/ic401765r | *Inorg. Chem.* 2013, 52, 14018−14027

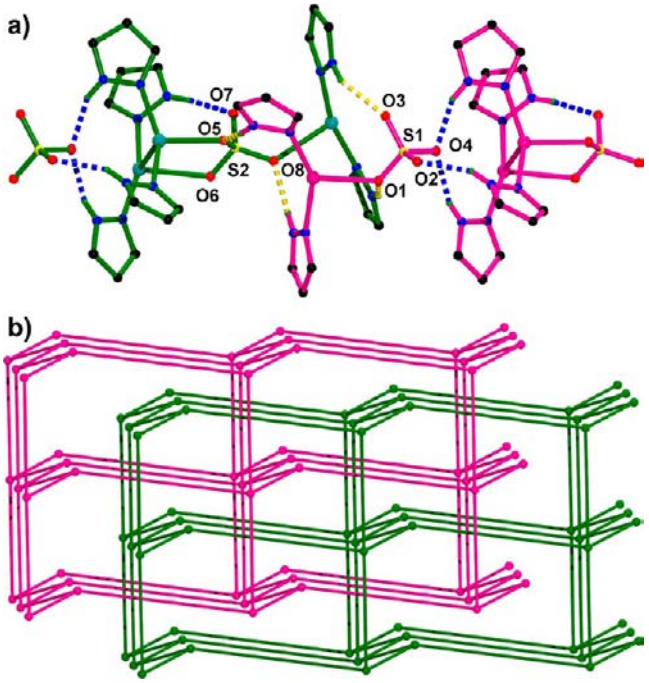

Figure 3. (a) The intra- (blue lines) and interframework (yellow lines) N−H···O hydrogen bonds and (b) (3,5)-connected hms topology of **1**.

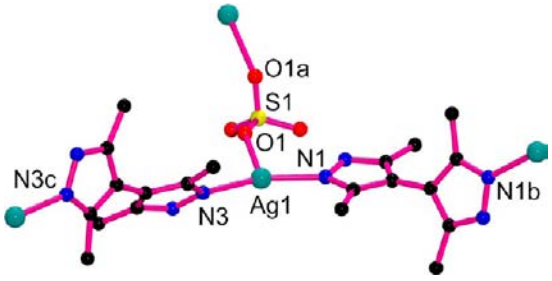

Figure 4. The coordination environments of Ag atoms in **2**. Symmetry codes: (a) $2 - x, 0.5 - y, z$; (b) $2.5 - x, 1 - y, z$; (c) $3 - x, 1 + y, -z$.

hydrophilic channel by SO_4^{2-} anions through O−H···O hydrogen bonds (Figure 6c). Along the *c* axis, the layers are tightened by other water (O1W) guests, which are involved in interlayer O−H···O and N−H···O hydrogen bonds with SO_4^{2-} anions and uncoordinated pyrazole -NH (N4) groups of H_2bpz (Table S2, Supporting Information).

Isomeric $[Ag(H_2bpz)]_n$ Chains. The $[Ag(H_2bpz)]_n$ subchains in **1** and **2** are conformational isomerisms, which address the conformational changes of H_2bpz ligand,[1e] in which the larger interpyrazole tilts and sole *trans* configuration of H_2bpz are mainly responsible for the helical chains in **2**. In regard to the similar T-shaped N_2O coordination environments of Ag(I) centers, three other $[Ag(H_2bpz)]_n$ isomers were noticed in 1D polymers $[Ag(H_2bpz)(X)]$ (X = NO_3^-, ClO_4^-, and $CF_3SO_3^-$),[5b,8a] which contain the same *trans*-H_2bpz as in **2** but display linear chains. These significant structural differences could be partly related to the different mutual orientations of two pyrazolyl rings around one metal center. In $CF_3SO_3^-$-, NO_3^--, and ClO_4^--containing chains, two pyrazolyl rings around one Ag(I) center exhibit not only *trans* configurations but also large tilting angles (58.9°, 63.5°, and 77.7°, respectively, Figure S2, Supporting Information); however, they exhibit *cis* and *trans* coexistent configurations with interplanar angles of 14.8°−67.0° in **1** and a *cis* arrangement with a tilt of 47.4° in **2**, thus rendering wavelike and helical chains in **1** and **2**, respectively.

Crystal Structure of 3. Complex **3** is a 3D polycatenating cationic framework with trigonal space group *P*3*c*1 and contains three independent Ag(I) ions, four H_2bpz ligands, and SO_4^{2-} and OH^- counteranions in the asymmetric unit. Different from **1** and **2**, the Ag atoms in **3** are tetrahedrally (Ag1) and angularly (Ag2 and Ag3) coordinated by pyrazole N atoms of different H_2bpz (Figure 7a). H_2bpz displays *cis* (N1- and N5-containing) and *trans* (N9- and N13-containing) exobidentate bridging fashions, which give short Ag···Ag separations for the former (9.542 and 9.373 Å) relative to the latter (9.878 and 9.923 Å), consistent with the situations in **1**. The angular coordination geometries of Ag2 (148.76°) and Ag3 (157.72°) atoms, as well as angular H_2bpz linker lead to the 2D grid layer structure of **3** (Figure 7b). The layer contains two symmetry-related left- and right-handed 4_1 helical chains along the *a* axis. And an interesting *meso*-helical chain is also formed in the layer along the *c* axis, which is unprecedented in $H_n$bpz$^{(n-2)}$-incorporated complexes.

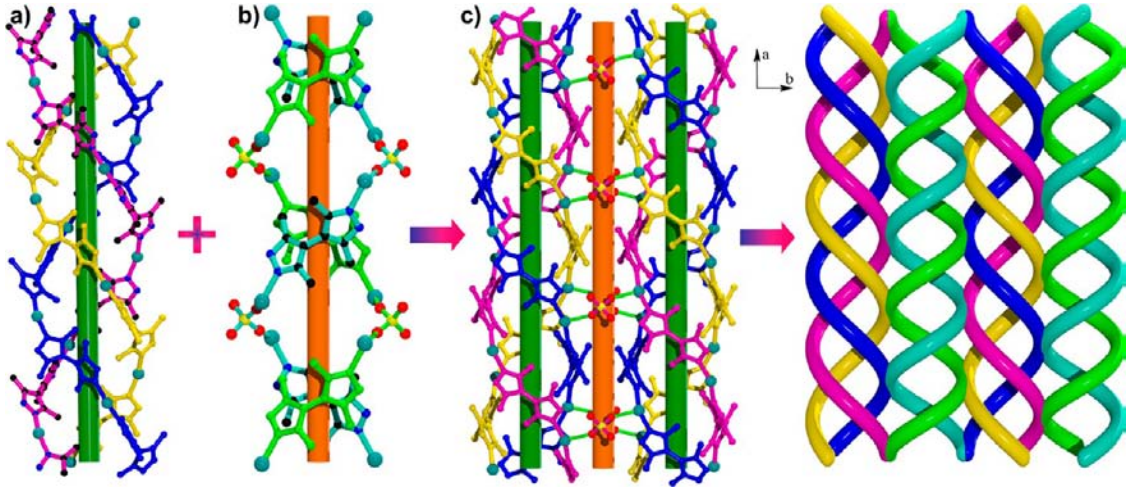

Figure 5. (a) Three-fold left-handed helical chain, (b) 2-fold right-handed helical chains, and (c) 2D achiral layer in **2**.

dx.doi.org/10.1021/ic401765r | *Inorg. Chem.* 2013, 52, 14018−14027

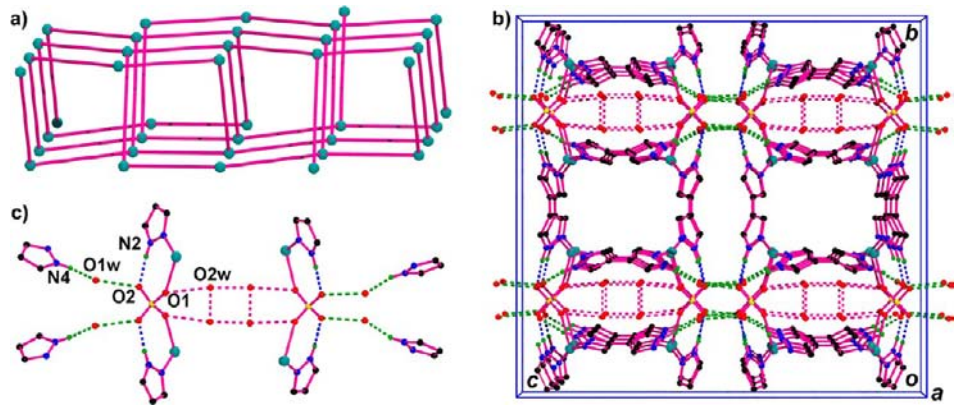

Figure 6. (a) Three-connected ths topological layer in **2**, and (b) 3D supramolecular structure of **2** formed by the intra- (purple lines) and interlayer (green lines) N−H···O and O−H···O hydrogen bonds (c, blue lines indicating the intramolecular hydrogen bonds; the methyl groups of H_2bpz were neglected).

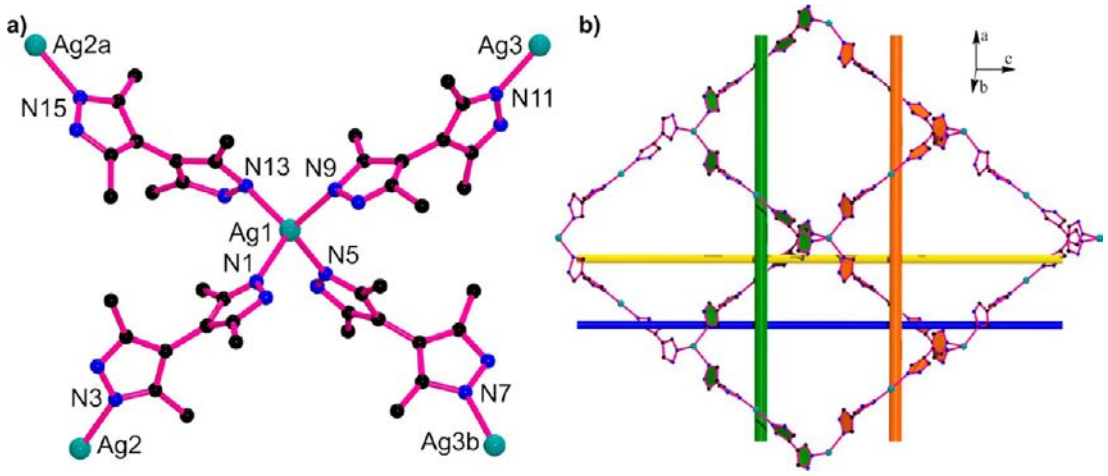

Figure 7. (a) The coordination environments of Ag atoms in **3**. Symmetry codes: (a) $2 - x + y, y, 0.5 + z$; (b) $1 - x + y, y, z - 0.5$. (b) Grid layer structure in **3**.

The most striking feature of **3** is the very uncommon type of 2D + 2D + 2D → 3D polycatenation in that three sets of layers exist and stack in three coplanar directions[23] of [100], [010], and [110] (Figure 8a,b), showing relative rotation angles of 60°. Each window in one layer is catenated by another layer with a diagonal−diagonal (d-d) type. The overall interpenetration mode in **3** can be described as d-d-d, with the density of catenation of (1/1/1).[23] To the best of our knowledge, only four similar polycatenating frameworks of **3**, which contain three sets of layers in three coplanar directions, are known.[24] However, the reported species display parallel−parallel−parallel (p-p-p) interpenetration modes and different densities of catenation of (2/2/2)[24a−c] and (2/4/4).[24d] Complex **3** represents the first example of 2D + 2D + 2D → 3D polycatenating framework by interlayer inclined interpenetration with d-d-d mode and density of catenation of (1/1/1). Such a unique interpenetration mode in **3** produces trigonal (3.5 × 3.5 Å^2, excluding van der Waals radii of the atoms) and hexagonal channels (4.4 × 4.4 Å^2) along the *c* axis, differing from the uniform trigonal channels in reported polycatenations containing three sets of layers.[24]

Interestingly, in **3**, three helices from three sets of layers converge to create a cavity with a diameter of ca. 5.7 Å (Figure 8c). The adjacent cavities are connected by the interstices (ca. 3.7 Å) generated between two helices, forming 2D pores parallel to the *ab* plane (Figure 8d), which are further bunched by the trigonal channels along the *c* axis into 3D pores. So the whole framework displays interesting 1D + 3D porous systems, in which the porous surfaces are mainly occupied by methyl and pyrazole -NH groups of H_2bpz. SO_4^{2-} anions occupy part of the trigonal channels and form N−H···O hydrogen bonds (Table S2, Supporting Information), leaving 23.7% voids in the framework.[16]

PXRD and TGA. The experimental PXRD patterns of **1**−**3** match with the simulated ones from the respective single-crystal structures (Figures S4 and S5, Supporting Information), confirming the phase purity. TGA of **1**−**3** indicates similar three-step weight losses under air atmosphere (Figure S6, Supporting Information). The first losses of 0.9%, 7.3%, and 5.0% from room temperature to 70, 135, and 130 °C for **1**, **2**, and **3**, respectively, correspond to the release of water guests (calcd values **1** 1.3%, **2** 7.2%, **3** 5.8%). Then **1**−**3** display thermostable plateaus up to 275, 300, and 250 °C, respectively. Further heating causes the decomposition of **1**−**3** into white Ag residues (**1**, found 31.2%, calcd 30.8%; **2**, found 29.2%; calcd 28.9%; **3**, found 27.2%, calcd 25.9%).

Luminescent Properties. Upon excitation at room temperature, solid **1**−**3** exhibit luminescence in blue region with centers at λ_{max} = 486 nm (λ_{ex} = 370 nm), 481 nm (λ_{ex} = 340 nm), and 409 nm (λ_{ex} = 336 nm), respectively (Figure 9).

dx.doi.org/10.1021/ic401765r | *Inorg. Chem.* 2013, 52, 14018−14027

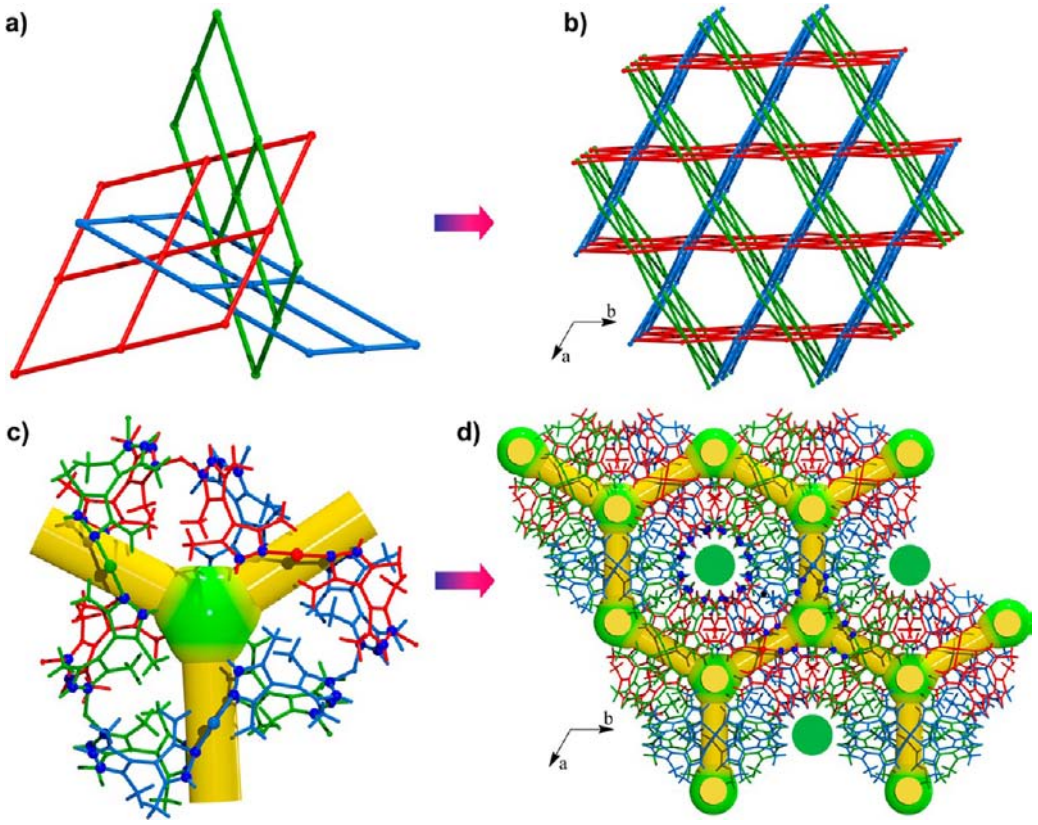

Figure 8. (a, b) Polycatenation of three sets of grids in different directions with d-d-d interpenetration mode, forming 1D + 3D porous systems (c, d) in **3**.

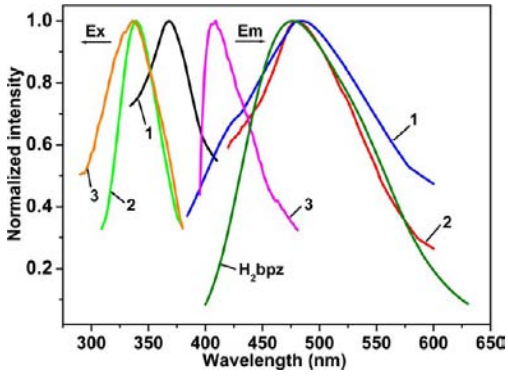

Figure 9. Solid-state excitation and emission spectra of **1**–**3** and H_2bpz at room temperature.

These bands can be tentatively assigned to ligand-centered fluorescent emissions of H_2bpz, which exhibits the maximum emission peak at 480 nm. Complexes **1** and **2** show similar emission spectra, which are related to the similar $[Ag(H_2bpz)]_n$ isomeric chain units in their structures. However, the broad emission band of **1** relative to **2** results from the mixture of metal-centered (MC) transitions supported by Ag(I)···Ag(I) interactions in **1**.[25] Compared with **1** and **2**, **3** displays high emission energy. This distinction, on one hand, could be attributed to the much larger interplanar dihedral angles (72.9–82.3°) of H_2bpz in **3** relative to those in **1** (51.8–70.3°) and **2** (57.7–70.0°), leading the lowest conjugated degrees of H_2bpz in **3** and shifting the emission band to higher energy.[26] On the other hand, it is probably due to dissimilar coordination environments around Ag(I) centers in **1** from **2** and **3**. The decay curves of **1**–**3** can be well fitted with two-exponential

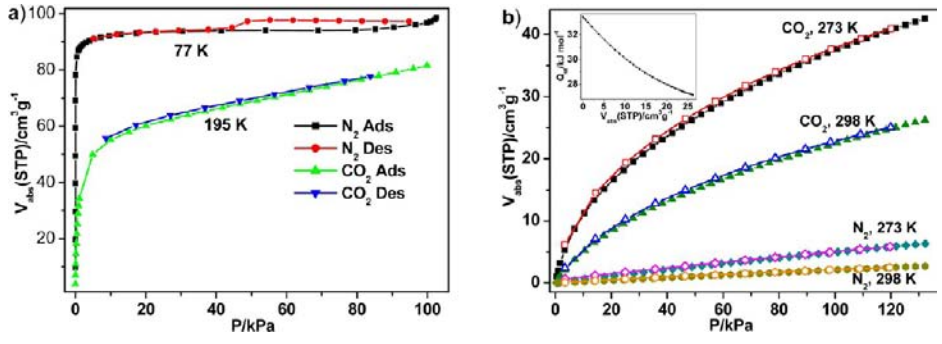

Figure 10. Gas sorption isotherms of **3** for N_2 and CO_2: (a) N_2 77 K and CO_2 195 K; (b) 273 and 298 K. The inset shows the CO_2 adsorption heat calculated according to the virial equation.

dx.doi.org/10.1021/ic401765r | *Inorg. Chem.* 2013, 52, 14018–14027

decay (Figures S7−9, Supporting Information), yielding approximate lifetimes of 1.27 and 5.38 ns for **1**, 0.76 and 3.03 ns for **2**, and 1.06 and 6.05 ns for **3**.

Sorption Properties. PCPs have been proposed as promising CO_2 adsorbents because of the well-defined porous structures and physisorption mechanism reducing their regenerating energy.[9a] While these materials are intensively focused on neutral and anionic frameworks, cationic architectures are much less investigated,[27] though cationic frameworks form strong interactions with CO_2 molecules.[27a−c] This prompts us to evaluate gas sorption properties of **3**. PXRD demonstrates the structural integrity of **3** after desolvation (Figure S5, Supporting Information). As shown in Figure 10a, the desolvated **3** shows reversible type-I sorption isotherms for N_2 at 77 K and CO_2 at 195 K. A BET surface area of 363 m^2 g^{-1} (Langmuir 404 m^2 g^{-1}) and a Dubinin−Astakhov pore volume of 0.14 cm^3 g^{-1} are calculated from N_2 adsorption curve. At 1 atm, N_2 and CO_2 loadings are 98.6 and 81.6 cm^3 (STP) g^{-1}, respectively. By the Horvath−Kawazoe model, a median pore width of 5.3 Å is obtained from CO_2 sorption isotherm at 195 K (Figure S10, Supporting Information).

At 273 and 298 K, **3** is almost nonadsorptive for N_2 (5.0 and 2.1 cm^3 (STP) g^{-1}) but exhibits moderate CO_2 uptakes of 37.6 and 22.6 cm^3 (STP) g^{-1} at 1 atm, respectively (Figure 10b). Under the same conditions of 298 K and 1 atm, this CO_2 sorption amount (4.4 wt %) in **3** is inferior to the value of 22.0 wt % in a recently reported zeolite-like zinc−tetrazole framework $[Zn(btz)]$[28] but superior to values in some Zn_4O-based frameworks with large pore dimensions (9.0−32.0 Å), such as MOF-177 (3.5 wt %),[29] SNU-70 (3.5 wt %),[30] and UMCM-1 (3.8 wt %),[31] implying that the small pore may be more attractive for CO_2 under low pressure.[32] The low-pressure adsorption capacities mainly rely on the heat of adsorption (Q_{st}).[33] So the Q_{st} of **3** for CO_2 was calculated according to the virial equation from the sorption isotherms at 273 and 298 K (Figure S11, Supporting Information). As shown in Figure 10b, the Q_{st} is 33.5 kJ mol^{-1} at zero loading, which greatly surpasses the zero-loading Q_{st} in cationic frameworks $[In_3O(3,3',5,5'\text{-azobenzenetetracarboxylate})_{1.5}(H_2O)_3]NO_3$ (28.5 kJ mol^{-1})[27a] and $[Cu_{24}(CN)_4(btc)_{12}(dabco)_9(H_2O)_6](NO_3)_8$ (23.2 kJ mol^{-1}).[27g] The Q_{st} slowly decreased with the increase of pressure, remaining up to 27.2 kJ mol^{-1} at maximum loading. This value even exceeds the zero-loading Q_{st} for CO_2 in some PCPs[27g,34] and BPL-carbon material (24.3 kJ mol^{-1}).[35] In the overall adsorption region, the mean Q_{st} is 30.4 kJ mol^{-1}. The high Q_{st} for CO_2 in **3** is attributed to the following crucial factors: first, the cationic feature of framework and extraframework anions (SO_4^{2-} and OH^-) induce strong electrostatic interactions with quadrupole CO_2 molecules.[27b,e] Second, Ag2 and Ag3 atoms in **3** are coordinatedly unsaturated due to their significantly angular coordination geometries (∠N−Ag−N = 148.76° and 157.72°); moreover, the exposed sites of these Ag atoms direct toward the inner of hexagonal 1D channel (Figure S3c, Supporting Information), which act as Lewis acidic sites to form strong affinity for CO_2 molecules. The uncoordinated pyrazole -NH groups of H_2bpz line on the porous surface and provide additional adsorption sites for CO_2 molecules. Third, the small pore formed due to methyl groups of H_2bpz promotes the overlap of potential fields from multiple sides of the pore walls, which strengthens framework−CO_2 interactions. Meanwhile, CO_2 molecules are forced to be close together in small pores, inducing CO_2−CO_2 interactions and providing moderate contributions for Q_{st}.[36] These factors lead to the overall high Q_{st} for CO_2 in **3**, distinguishing it from the amine-functionalized framework $H_3[(Cu_4Cl_3)(BTTri)_8]$-ethylenediamine,[37] in which, due to large pore sizes, the Q_{st} decreases abruptly to about 25 kJ mol^{-1} (0.5 atm) with increasing CO_2 loadings despite its high initial Q_{st} (90 kJ mol^{-1}). By contrast, the relatively low Q_{st} (18−22 kJ mol^{-1}, 0−1 atm) for CO_2 was also observed in a (10,3)-*a* framework $[Ag_2(bpz)]$,[13a] which features a neutral network, linearly coordinated Ag(I) centers, and no uncoordinated -NH groups in the pores.

In separation processes, the selectivity for different components in mixtures is a critical indicator for adsorbent materials. Herein, analysis of the single-component isotherms of CO_2 and N_2 at 298 K using the ideal adsorbed solution theory (IAST) gives the multicomponent adsorption curves and selectivities for CO_2/N_2 mixtures (Figures S12 and S13, Supporting Information). The predicted adsorption selectivities in **3** for CO_2/N_2 with mole ratios of 50:50 and 15:85 as a function of total bulk pressure are shown in Figure 11.

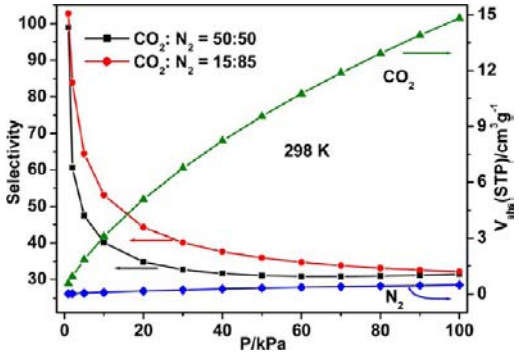

Figure 11. IAST adsorption selectivities of **3** for CO_2 over N_2 at different compositions and isotherms at 298 K for equimolar mixtures.

Complex **3** exhibits very high initial CO_2/N_2 selectivities (∼100) for two different mixture compositions, and then the selectivities decrease with increasing pressure. Except in the low-pressure region, the selectivities rise with reduced CO_2 contents from 50% to 15%, which resemble the results in some reported PCPs.[38] For the case of 15% CO_2 in the mixture, a typical flue gas composition from coal-fired power plants,[9a] the CO_2/N_2 selectivity in **3** is 32 at 1 atm. This is comparable to the reported values at 298 K and 1 atm in Ni-MOF-74 (30)[32] and ZIF-78 (30)[39] but much higher than the experimental values in zeolite 4A (19) and zeolite13X (18) (298 K and 1 atm).[40] Even for equimolar mixtures, the selectivities (33−99) are considerably higher compared with other PCPs, such as $[Zn(BDC\text{-}R)(TED)_{0.5}]$ (R= -H, -OH, and -NH_2) (3−17)[34a] and Cu-BTC (20−25)[41] at 298 K and 0−1 atm conditions.

The excellent CO_2/N_2 selectivities at 298 K in **3** result from the various interactions among CO_2 and N_2 with framework. In **3**, the cationic framework, extra-framework anions, methyl groups, and pyrazole -NH groups of H_2bpz and coordinatedly unsaturated Ag(I) centers make the framework highly polar, generating stronger affinity for CO_2 than N_2 because CO_2 has a larger quadrupole moment (−4.3 B) than N_2 (−1.4 B). It is worth mentioning that the stability toward water is one of the main challenges in applying PCPs as CO_2 adsorbents.[9a] Besides good stabilization of **3** in air, water, and common organic solvents, PXRD demonstrates that **3** holds framework integrity after immersion in HNO_3 (pH = 2) aqueous solution for 24 h (Figure S5, Supporting Information). These results suggest that

dx.doi.org/10.1021/ic401765r | Inorg. Chem. 2013, 52, 14018−14027

3 is a promising candidate for CO_2 capture from industrial flue gas, which contains a certain amount of moisture.

For a better understanding of sorption properties, density contours were calculated to identify favorable binding sites for CO_2 adsorption in **3** by GCMC simulations at 298 K under pressures 0.1 and 100 kPa (Figure S14, Supporting Information). It shows that at low pressure (0.1 kPa), CO_2 molecules are primarily adsorbed in the regions of uncoordinated -NH groups and methyl groups of H_2bpz in 1D channel. At high pressure (100 kPa), the binding sites are mostly located in the vicinity of coordinatedly unsaturated Ag(I) centers in the 1D channel and SO_4^{2-} and methyl groups of H_2bpz in the 3D pores. In addition, at the same pressure 100 kPa, the simulated adsorption heat of 27.7 kJ mol^{-1} for CO_2 in **3** is consistent with the calculated value (27.5 kJ mol^{-1}) from experimental data.

CONCLUSIONS

In summary, we have constructed three CPs employing Ag_2SO_4 and H_2bpz ligand. This work demonstrates that the variations of reaction solvents and temperatures are critical to the assemblies of CPs in some systems. The changeable interpyrazole tilting angles and various coordination configurations of H_2bpz lead to $[Ag(H_2bpz)]_n$ isomers wherein *cis*- and *trans*-H_2bpz contribute to wavelike chains in **1** and *trans*-H_2bpz forms helical chains in **2**. As expected, SO_4^{2-} anion plays an important role in eventual frameworks, which acts as a linker to bridge the chains in **1** and **2** into 3D and 2D structures, respectively, while being a counteranion in **3**. Complexes **1** and **2** are structural isomers, in which **1** exhibits a 2-fold interpenetrated (3,5)-connected hms net, and **2** is a 3-connected ths net containing interesting 3-fold and 2-fold heterochiral helical chains. Complex **3** is a rare 2D + 2D + 2D → 3D polycatenating porous framework based on interpenetration of three sets of layers, featuring an unprecedented d-d-d interpenetration mode with the density of catenation of (1/1/1). Such an unusual polycatenation contributes to intriguing self-assembly chemistry. Complexes **1**−**3** exhibit solid-state luminescence with different emission energies due to the diverse coordination environments of Ag(I) centers and different interplanar dihedral angles of H_2bpz in them. The cationic framework, SO_4^{2-} and OH^- anions, and small-sized pores decorated by coordinatedly unsaturated Ag(I) centers and methyl and -NH groups of H_2bpz offer highly polar pores in **3**, which lead to high heat of sorption for CO_2 and high CO_2/N_2 selectivity. In addition, **3** displays outstanding resistance toward water. The extendable work will construct chemically stable materials through employing a variety of bipyrazole ligands with different functionalized groups.

ASSOCIATED CONTENT

Supporting Information

X-ray crystallographic data in CIF format, additional structural figures, FTIR, TGA, PXRD patterns, luminescence decay curves of **1**−**3**, the detailed calculations on sorption, and bond length and angle, hydrogen bond, and partial charge tables. This material is available free of charge via the Internet at http://pubs.acs.org.

AUTHOR INFORMATION

Corresponding Author

*E-mail: lhou2009@nwu.edu.cn (L.H.).

Notes

The authors declare no competing financial interest.

ACKNOWLEDGMENTS

We are grateful for financial support from the NSF of China (Grants 21001088, 91022004, 2093115, and 21371142), NSF of Shaanxi province (Grants 2013KJXX-26 and 13JS114), and the Australian Research Council Discovery Project DP1096948.

REFERENCES

(1) (a) O'Keeffe, M.; Yaghi, O. M. *Chem. Rev.* **2012**, *112*, 675−702. (b) Zhang, J.-P.; Zhang, Y.-B.; Lin, J.-B.; Chen, X.-M. *Chem. Rev.* **2012**, *112*, 1001−1033. (c) Natarajan, S.; Mahata, P. *Chem. Soc. Rev.* **2009**, *38*, 2304−2318. (d) Yin, Z.; Wang, Q.-X.; Zeng, M.-H. *J. Am. Chem. Soc.* **2012**, *134*, 4857−4863. (e) Hennigar, T. L.; MacQuarrie, D. C.; Losier, P.; Rogers, R. D.; Zaworotko, M. J. *Angew. Chem., Int. Ed. Engl.* **1997**, *36*, 972−973.

(2) (a) Zhang, J.; Wojtas, L.; Larsen, R. W.; Eddaoudi, M.; Zaworotko, M. *J. Am. Chem. Soc.* **2009**, *131*, 17040−17041. (b) Li, C.-P.; Yu, Q.; Chen, J.; Du, M. *Cryst. Growth Des.* **2010**, *10*, 2650−2660. (c) Luo, L.; Chen, K.; Liu, Q.; Lu, Y.; Okamura, T.-a.; Lv, G.-C.; Zhao, Y.; Sun, W.-Y. *Cryst. Growth Des.* **2013**, *13*, 2312−2321. (d) Sun, D.; Ke, Y.; Collins, D. J.; Lorigan, G. A.; Zhou, H.-C. *Inorg. Chem.* **2007**, *46*, 2725−2734.

(3) (a) Li, C.-P.; Du, M. *Chem. Commun.* **2011**, *47*, 5958−5972. (b) Yang, G.-P.; Hou, L.; Ma, L.-F.; Wang, Y.-Y. *CrystEngComm* **2013**, *15*, 2561−2578. (c) Chen, M.; Lu, Y.; Fan, J.; Lv, G.-C.; Zhao, Y.; Zhang, Y.; Sun, W.-Y. *CrystEngComm* **2012**, *14*, 2015−2023. (d) Xiao, J.; Liu, B.-Y.; Wei, G.; Huang, X.-C. *Inorg. Chem.* **2011**, *50*, 11032−11038. (e) Cui, P.; Ren, L.; Chen, Z.; Hu, H.; Zhao, B.; Shi, W.; Cheng, P. *Inorg. Chem.* **2012**, *51*, 2303−2310. (f) Lan, Y.-Q.; Jiang, H.-L.; Li, S.-L.; Xu, Q. *Inorg. Chem.* **2012**, *51*, 7484−7491. (g) Song, F.; Wang, C.; Falkowski, J. M.; Ma, L.; Lin, W. *J. Am. Chem. Soc.* **2012**, *132*, 15390−15398.

(4) (a) Khlobystov, A. N.; Blake, A. J.; Champness, N. R.; Lemenovskii, D. A.; Majouga, A. G.; Zyk, N. V.; Schröder, M. *Coord. Chem. Rev.* **2001**, *222*, 155−192. (b) May, L. J.; Shimizu, G. K. H. *Chem. Mater.* **2005**, *17*, 217−220. (c) Liu, S. Q.; Kuroda-Sowa, T.; Konaka, H.; Suenaga, Y.; Maekawa, M.; Mizutani, T.; Ning, G. L.; Munakata, M. *Inorg. Chem.* **2005**, *44*, 1031−1036. (d) Ling, Y.; Zhai, F.-P.; Deng, M.-L.; Wu, D.; Chen, Z.-X.; Liu, X.-F.; Zhou, Y.-M. *CrystEngComm* **2012**, *14*, 1425−1431. (e) Tăbăcaru, A.; Pettinari, C.; Marchetti, F.; Nicola, C. d.; Domasevitch, K. V.; Galli, S.; Masciocchi, N.; Scuri, S.; Grappasonni, I.; Cocchioni, M. *Inorg. Chem.* **2012**, *51*, 9775−9788. (f) Tsukuda, T.; Kawase, M.; Dairiki, A.; Matsumoto, K.; Tsubomura, T. *Chem. Commun.* **2010**, *46*, 1905−1907.

(5) (a) Young, A. G.; Hanton, L. R. *Coord. Chem. Rev.* **2008**, *252*, 1346−1386. (b) Domasevitch, K. V.; Boldog, I.; Rusanov, E. B.; Hunger, J.; Blaurock, S.; Schröder, M.; Sieler, J. *Z. Anorg. Allg. Chem.* **2005**, *631*, 1095−1100. (c) Cui, L.-N.; Hu, K.-Y.; Jin, Q.-H.; Li, Z.-F.; Wu, J.-Q.; Zhang, C.-L. *Polyhedron* **2011**, *30*, 2253−2259. (d) Yang, G.; Wang, Y.-L.; Li, J.-P.; Zhu, Y.; Wang, S.-M.; Hou, H.-W.; Fan, Y.-T.; Ng, S. W. *Eur. J. Inorg. Chem.* **2007**, 714−719. (e) Wang, Y.; Ding, B.; Cheng, P.; Liao, D.-Z.; Yan, S.-P. *Inorg. Chem.* **2007**, *46*, 2002−2010. (f) Santillan, G. A.; Carrano, C. J. *Dalton Trans.* **2009**, 6599−6605. (g) Chen, H.-C.; Hu, H.-L.; Chan, Z.-K.; Yeh, C.-W.; Jia, H.-W.; Wu, C.-P.; Chen, J.-D.; Wang, J.-C. *Cryst. Growth Des.* **2007**, *7*, 698−704.

(6) (a) Lucas, J. S.; Uebler, J. W.; LaDuca, R. L. *CrystEngComm* **2013**, *15*, 860−866. (b) Darling, K.; Ouellette, W.; Prosvirin, A.; Freund, S.; Dunbar, K. R.; Zubieta, J. *Cryst. Growth Des.* **2012**, *12*, 2662−2672. (c) Hou, L.; Zhang, W.-X.; Zhang, J.-P.; Xue, W.; Zhang, Y.-B.; Chen, X.-M. *Chem. Commun.* **2010**, *46*, 6311−6313.

(7) Boldog, I.; Rusanov, E. B.; Chernega, A. N.; Sieler, J.; Domasevitch, K. V. *J. Chem. Soc., Dalton Trans.* **2001**, 893−897.

(8) (a) Boldog, I.; Rusanov, E. B.; Chernega, A. N.; Sieler, J.; Domasevitch, K. V. *Polyhedron* **2001**, *20*, 887−897. (b) Xie, Y.-M.;

Zhao, Z.-G.; Wu, X.-Y.; Zhang, Q.-S.; Chen, L.-J.; Wang, F.; Chen, S.-C.; Lu, C.-Z. *J. Solid State Chem.* **2008**, *181*, 3322−3326.
(9) (a) Sumida, K.; Rogow, D. L.; Mason, J. A.; McDonald, T. M.; Bloch, E. D.; Herm, Z. R.; Bae, T.-H.; Long, J. R. *Chem. Rev.* **2012**, *112*, 724−781. (b) Liu, J.; Thallapally, P. K.; McGrail, B. P.; Brown, D. R.; Liu, J. *Chem. Soc. Rev.* **2012**, *41*, 2308−2322. (c) Li, J.-R.; Ma, Y.; McCarthy, M. C.; Sculley, J.; Yu, J.; Jeong, H.-K.; Balbuena, P. B.; Zhou, H.-C. *Coord. Chem. Rev.* **2011**, *255*, 1791−1823. (d) Kanoo, P.; Ghosh, A. C.; Cyriac, S. T.; Maji, T. K. *Chem.—Eur. J.* **2012**, *18*, 237−244. (e) Hou, C.; Liu, Q.; Fan, J.; Zhao, Y.; Wang, P.; Sun, W.-Y. *Inorg. Chem.* **2012**, *51*, 8402−8408. (f) Hu, T.-L.; Tao, Y.; Chang, Z.; Bu, X.-H. *Inorg. Chem.* **2011**, *50*, 10994−11003. (g) Lin, Z.-J.; Huang, Y.-B.; Liu, T.-F.; Li, X.-Y.; Cao, R. *Inorg. Chem.* **2013**, *52*, 3127−3132. (h) Lin, Z.-J.; Liu, T.-F.; Huang, Y.-B.; Lü, J.; Cao, R. *Chem.—Eur. J.* **2012**, *18*, 7896−7902.
(10) (a) Liang, Z.; Marshall, M.; Chaffee, A. L. *Energy Fuels* **2009**, *23*, 2785−2789. (b) Li, Y.; Yang, R. T. *Langmuir* **2007**, *23*, 12937−12944. (c) Greathouse, J. A.; Allendorf, M. D. *J. Am. Chem. Soc.* **2006**, *128*, 10678−10679.
(11) (a) Tăbăcaru, A.; Pettinari, C.; Timokhin, I.; Marchetti, F.; Carrasco-Marín, F.; Maldonado-Hódar, F. J.; Galli, S.; Masciocchi, N. *Cryst. Growth Des.* **2013**, *13*, 3087−3097. (b) Montoro, C.; Linares, F.; Procopio, E. Q.; Senkovska, I.; Kaskel, S.; Galli, S.; Masciocchi, N.; Barea, E.; Navarro, J. A. R. *J. Am. Chem. Soc.* **2011**, *133*, 11888−11891. (c) Choi, H. J.; Dincă, M.; Dailly, A.; Long, J. R. *Energy Environ. Sci.* **2010**, *3*, 117−123.
(12) Vaidhyanathan, R.; Iremonger, S. S.; Shimizu, G. K. H.; Boyd, P. G.; Alavi, S.; Woo, T. K. *Science* **2010**, *330*, 650−653.
(13) (a) Zhang, J.-P.; Kitagawa, S. *J. Am. Chem. Soc.* **2008**, *130*, 907−917. (b) Zhang, J.-P.; Horike, S.; Kitagawa, S. *Angew. Chem., Int. Ed.* **2007**, *46*, 889−892.
(14) Mosby, W. L. *J. Chem. Soc.* **1957**, 3997−4003.
(15) Sheldrick, G. M. *SHELXL*, version 6.12; Bruker Analytical Instrumentation, Madison, WI, 2000.
(16) Spek, A. L. *J. Appl. Crystallogr.* **2003**, *36*, 7−13.
(17) *Accelrys, Materials Studio Getting Started*, release 5.0; Accelrys Software, Inc., San Diego, CA, 2009.
(18) Hirotani, A.; Mizukami, K.; Miura, R.; Takaba, H.; Miya, T.; Fahmi, A.; Stirling, A.; Kubo, M.; Miyamoto, A. *Appl. Surf. Sci.* **1997**, *120*, 81−84.
(19) (a) Xie, Y.-M.; Liu, J.-H.; Wu, X.-Y.; Zhao, Z.-G.; Zhang, Q.-S.; Wang, F.; Chen, S.-C.; Lu, C.-Z. *Cryst. Growth Des.* **2008**, *8*, 3914−3916. (b) Li, D.-Q.; Hou, L.; Ng, S. W. *Acta Crystallogr.* **2007**, *E63*, m1864.
(20) Blatov, V. A. Topos, 2007, http://www.topos.ssu.samara.ru.
(21) (a) Gao, C.; Liu, S.; Xie, L.; Ren, Y.; Cao, J.; Sun, C. *CrystEngComm* **2007**, *9*, 545−547. (b) Hou, L.; Zhang, J.-P.; Chen, X.-M. *Cryst. Growth Des.* **2009**, *9*, 2415−2419. (c) Han, Z.-B.; Liang, Y.-F.; Zhou, M.; Zhang, Y.-R.; Li, L.; Tong, J. *CrystEngComm* **2012**, *14*, 6952−6956. (d) He, H.; Dai, F.; Sun, D. *Dalton Trans.* **2009**, 763−766.
(22) Barnett, S. A.; Blake, A. J.; Champness, N. R.; Wilson, C. *Chem. Commun.* **2002**, 1640−1641.
(23) Carlucci, L.; Ciani, G.; Proserpio, D. M. *Coord. Chem. Rev.* **2003**, *246*, 247−289.
(24) (a) Chen, B.; Jiang, F.; Han, L.; Wu, B.; Yuan, D.; Wu, M.; Hong, M. *Inorg. Chem. Commun.* **2006**, *9*, 371−374. (b) Wang, S.; Wang, D.; Dou, J.; Li, A. *Acta Crystallogr.* **2010**, *C66*, m141−m144. (c) Zhuang, W. J.; Zheng, X. J.; Li, L. C.; Liao, D. Z.; Ma, H.; Jin, L. P. *CrystEngComm* **2007**, *9*, 653−667. (d) Carlucci, L.; Ciani, G.; Proserpio, D. M.; Rizzato, S. *CrystEngComm* **2003**, *5*, 190−199.
(25) (a) Yam, V. W.-W.; Lo, K. K.-W. *Chem. Soc. Rev.* **1999**, *28*, 323−334. (b) Eberhard, J.; Stoll, I.; Brockhinke, R.; Neumann, B.; Stammler, H.; Riefer, A.; Rauls, E.; Schmidt, W. G.; Mattay, J. *CrystEngComm* **2013**, *15*, 4225−4248. (c) Li, N.-Y.; Ren, Z.-G.; Liu, D.; Yuan, R.-X.; Wei, L.-P.; Zhang, L.; Li, H.-X.; Lang, J.-P. *Dalton Trans.* **2010**, *39*, 4213−4222.
(26) Lestari, W. W.; Lönnecke, P.; Sárosi, M. B.; Streit, H. C.; Adlung, M.; Wickleder, C.; Handke, M.; Einicke, W.-D.; Gläser, R.; Hey-Hawkins, E. *CrystEngComm* **2013**, *15*, 3874−3884.
(27) (a) Moellmer, J.; Celler, E. B.; Luebke, R.; Cairns, A. J.; Staudt, R.; Eddaoudi, M.; Thommes, M. *Microporous Mesoporous Mater.* **2010**, *129*, 345−353. (b) Jiang, J. *AIChE J.* **2009**, *55*, 2422−2432. (c) Maji, T. K.; Matsuda, R.; Kitagawa, S. *Nat. Mater.* **2007**, *6*, 142−148. (d) Chandler, B. D.; Cramb, D. T.; Shimizu, G. K. H. *J. Am. Chem. Soc.* **2006**, *128*, 10403−10412. (e) Li, D.; Kaneko, K. *Chem. Phys. Lett.* **2001**, *335*, 50−56. (f) Kondo, A.; Chinen, A.; Kajiro, H.; Nakagawa, T.; Kato, K.; Takata, M.; Hattori, Y.; Okino, F.; Ohba, T.; Kaneko, K.; Kanoh, K. *Chem.—Eur. J.* **2009**, *15*, 7549−7553. (g) Lian, T.-T.; Chen, S.-M.; Wang, F.; Zhang, J. *CrystEngComm* **2013**, *15*, 1036−1038.
(28) Cui, P.; Ma, Y.-G.; Li, H.-H.; Zhao, B.; Li, J.-R.; Cheng, P.; Balbuena, P. B.; Zhou, H.-C. *J. Am. Chem. Soc.* **2012**, *134*, 18892−18895.
(29) Millward, A. R.; Yaghi, O. M. *J. Am. Chem. Soc.* **2005**, *127*, 17998−17999.
(30) Prasad, T. K.; Suh, M. P. *Chem.—Eur. J.* **2012**, *18*, 8673−8680.
(31) Yazaydin, A. Ö.; Snurr, R. Q.; Park, T.-H.; Koh, K.; Liu, J.; LeVan, M. D.; Benin, A. I.; Jakubczak, P.; Lanuza, M.; Galloway, D. B.; Low, J. J.; Willis, R. R. *J. Am. Chem. Soc.* **2009**, *131*, 18198−18199.
(32) Rowsell, J. L. C.; Millward, A. R.; Park, K. S.; Yaghi, O. M. *J. Am. Chem. Soc.* **2004**, *126*, 5666−5667.
(33) Frost, H.; Düren, T.; Snurr, R. Q. *J. Phys. Chem. B* **2006**, *110*, 9565−9570.
(34) (a) Zhang, Z.; Liu, J.; Li, Z.; Li, J. *Dalton Trans.* **2012**, *41*, 4232−4238. (b) Wade, C. R.; Dincă, M. *Dalton Trans.* **2012**, *41*, 7931−7938. (c) Tan, Y.-X.; He, Y.-P.; Zhang, J. *Cryst. Growth Des.* **2012**, *12*, 2468−2471.
(35) D'Alessandro, D. M.; Smit, B.; Long, J. R. *Angew. Chem., Int. Ed.* **2010**, *49*, 6058−6082.
(36) Yang, Q.; Zhong, C.; Chen, J.-F. *J. Phys. Chem. C* **2008**, *112*, 1562−1569.
(37) Demessence, A.; D'Alessandro, D. M.; Foo, M. L.; Long, J. R. *J. Am. Chem. Soc.* **2009**, *131*, 8784−8786.
(38) (a) Bae, Y.-S.; Farha, O. K.; Hupp, J. T.; Snurr, R. Q. *J. Mater. Chem.* **2009**, *19*, 2131−2134. (b) Bae, Y.-S.; Mulfort, K. L.; Frost, H.; Ryan, P.; Punnathanam, S.; Broadbelt, L. J.; Hupp, J. T.; Snurr, R. Q. *Langmuir* **2008**, *24*, 8592−8598.
(39) Phan, A.; Doonan, C. J.; Uribe-Romo, F. J.; Knobler, C. B.; O'Keefe, M.; Yaghi, O. M. *Acc. Chem. Res.* **2010**, *43*, 58−67.
(40) Siriwardance, R. V.; Shen, M.-S.; Fisher, E. P.; Poston, J. A. *Energy Fuels* **2011**, *15*, 279−284.
(41) Yang, Q.; Xue, C.; Zhong, C.; Chen, J.-F. *AIChE J.* **2007**, *53*, 2832−2840.